AD

CONTRACT REPORT ARBRL-CR-00520

MODIFICATION OF THE η-INVARIANT CODE FOR APPLICATION ON A MODULAR GRID NETWORK

Prepared by

University of Iowa
RR1 Box 22
Maxwell, Iowa 50161

November 1983

US ARMY ARMAMENT RESEARCH AND DEVELOPMENT CENTER
BALLISTIC RESEARCH LABORATORY
ABERDEEN PROVING GROUND, MARYLAND

Destroy this report when it is no longer needed.
Do not return it to the originator.

Additional copies of this report may be obtained from the National Technical Information Service, U. S. Department of Commerce, Springfield, Virginia 22161.

The findings in this report are not to be construed as an official Department of the Army position, unless so designated by other authorized documents.

The use of trade names or manufacturers' names in this report does not constitute indorsement of any commercial product.

UNCLASSIFIED

SECURITY CLASSIFICATION OF THIS PAGE *(When Data Entered)*

REPORT DOCUMENTATION PAGE		READ INSTRUCTIONS BEFORE COMPLETING FORM
1. REPORT NUMBER CONTRACT REPORT ARBRL-CR-00520	2. GOVT ACCESSION NO.	3. RECIPIENT'S CATALOG NUMBER
4. TITLE *(and Subtitle)* MODIFICATION OF THE η-INVARIANT CODE FOR APPLICATION ON A MODULAR GRID NETWORK		5. TYPE OF REPORT & PERIOD COVERED Final 6. PERFORMING ORG. REPORT NUMBER
7. AUTHOR(s) Richard G. Hindman		8. CONTRACT OR GRANT NUMBER(s) DAAG29-81-D-0100
9. PERFORMING ORGANIZATION NAME AND ADDRESS University of Iowa RR1 Box 22 Maxwell, Iowa 50161		10. PROGRAM ELEMENT, PROJECT, TASK AREA & WORK UNIT NUMBERS RDT&E 1L161102AH43
11. CONTROLLING OFFICE NAME AND ADDRESS US Army AMCCOM, ARDC Ballistic Research Laboratory, ATTN: DRSMC-BLA-S(A) Aberdeen Proving Ground, MD 21005		12. REPORT DATE November 1983 13. NUMBER OF PAGES 35
14. MONITORING AGENCY NAME & ADDRESS*(if different from Controlling Office)*		15. SECURITY CLASS. *(of this report)* Unclassified 15a. DECLASSIFICATION/DOWNGRADING SCHEDULE

16. DISTRIBUTION STATEMENT *(of this Report)*

Approved for public release, distribution unlimited.

17. DISTRIBUTION STATEMENT *(of the abstract entered in Block 20, if different from Report)*

18. SUPPLEMENTARY NOTES

This work was performed under the direction of the Aerodynamics Research Branch, Launch and Flight Division, DRDAR-BLL, Mr. Charles J. Nietubicz, Contracting Officer's Technical Representative.

19. KEY WORDS *(Continue on reverse side if necessary and identify by block number)*

Navier-Stokes Solver
Finite Difference
Approximate Factorization
Hollow Projectiles
Computational Grids

20. ABSTRACT *(Continue on reverse side if necessary and identify by block number)*

Extensive modifications to the η-Invariant code for computation of tubular projectile flowfields are reported. An efficient modular grid network is implemented consisting of a find mesh near the projectile, a coarse mesh on the interior of the projectile, and a coarse mesh on the exterior region. The conventional implicit factored integration scheme in "delta form" is modified to allow for block tridiagonal inversion along a line which crosses from one mesh to another. Special intermesh operators are derived for implementation of this

DD FORM 1 JAN 73 1473 EDITION OF 1 NOV 65 IS OBSOLETE

UNCLASSIFIED

SECURITY CLASSIFICATION OF THIS PAGE *(When Data Entered)*

20. ABSTRACT (Continued).

idea at the intermesh points and their immediate neighbors. Complex applications topology of various block inversions are discussed in detail.

TABLE OF CONTENTS

LIST OF ILLUSTRATIONS

I. INTRODUCTION

The purpose of this effort was to modify an existing computer code (Ref. 1) for more efficient computation of viscous flowfields in and about hollow projectile shapes. (See Fig. 1.) The existing code solves the axisymmetric thin-layer equations on domains consisting of a single element or module. A typical grid for a problem of this type is shown in Fig. 2. Grids of this type suffer from several problems. First of all, skewness problems in such a grid prevent accurate solutions and can even lead to instabilities. Secondly, computed inefficiency exists due to the concentration of points where they are not needed. Finally, this type of grid results in severe and undesirable gradients in geometric parameters near the inflow boundary intersection with the projectile axis. Of course these grid problems can be quite detrimental to the quality of the computed solution and can result in excessive CPU time requirements.

The method chosen to eliminate these grid problems was to develop a modular grid system. The schematic of such a system is shown in Fig. 3. A grid system of this type has several attractive features. First, points are concentrated where they are needed. For example, sufficient refinement is obtained in the boundary-layer regions without forced refinement where it is not needed. Also,the number of vertical points in Region 2 is independent of that in Region 3. This prevents the wasted computation on the inside of the projectile that existed for the original grid. Secondly, the geometric parameters are well behaved in the corner where the inflow boundary intersects the projectile centerline. In addition, this type of grid system virtually eliminates skewness problems.

There are some disadvantages of this type of grid system, also. First, it requires grid generation, flow solution, output, etc., for each distinct region rather than just one domain. In addition, the interfaces between the distinct regions of the grid require special consideration since the separate grids need not have continuous mappings across these interfaces. For example, between Regions 1 and 2 the grid suddenly changes from a very fine mesh to a coarse one. As a result of these special considerations, the coding logic for performing the block-tridiagonal inversions through these interfaces becomes very complex and is compounded further by the fact that the strong-conservation-law form of the governing fluid equations is employed. This fact will become obvious in the development of the required interface operators.

The fundamental notion employed in this work is that second-order accurate central-difference approximations for first and second derivatives on a uniformly spaced grid in computational space may be replaced by second-order accurate approximations on an unequally spaced grid in computational space without compromising the tridiagonal structure of the difference operator. This is demonstrated in the following section.

II. CONCEPT TESTING

The notion of employing finite-difference approximations to an unequally spaced grid in computational space is tested on a one-dimensional model problem governed by the nonlinear viscous Burgers' equation

$$\frac{\partial u}{\partial t} + \frac{\partial f}{\partial x} = \mu \frac{\partial^2 u}{\partial x^2}, \qquad f = \frac{u^2}{2} \tag{1}$$

subject to the boundary conditions

$$u(0,t) = 1$$

$$u(1,t) = 0$$

and the initial conditions

$$u(x,0) = \begin{cases} 1 , & x = 0 \\ 0 , & 0 < x \leq 1 \end{cases}$$

The exact steady-state solution to this problem is

$$u = \hat{u} \tanh\left[\frac{\hat{u}}{2\mu} (1 - x)\right]$$

where $\hat{u}$ solves the transcendental equation

$$\frac{\hat{u} - 1}{\hat{u} + 1} = e^{-\hat{u}/\mu}$$

This problem was chosen for several reasons. First, the exact solution is known; thus, a precise measure of the error generated by the finite-difference scheme is known. Second, for sufficiently small values of μ, a steep gradient in the solution exists near the right boundary of the domain. (See Fig. 4.) This behavior is similar to that which exists in a boundary-layer region. Thus the domain can be partitioned into two grids: a fine mesh near the right boundary and a coarse mesh elsewhere. Since μ can be adjusted to position the steep gradient either completely within the fine mesh or so that it crosses the intermesh boundary, the required intermesh operators can be severely tested with this problem.

Equation (1) must be transformed to computational space according to the mapping $\tau = t$, $\xi = \xi(x)$. Note that actually two mappings are employed, one for the fine grid and one for the coarse grid. The mapped equation is

$$\frac{\partial u}{\partial \tau} + \xi_x \frac{\partial f}{\partial \xi} = \mu \xi_x^2 \left(\frac{\partial^2 u}{\partial \xi^2} - \xi_{xx} \frac{\partial u}{\partial \xi} \right)$$

Consistent with the tubular projectile code, the Beam-Warming implicit numerical integration scheme in delta form (Ref. 2) is used to solve this equation. The scheme is expressed as

$$\left\{1 - \beta\Delta\tau\left[\frac{\mu}{x_\xi^2}\frac{\partial^2}{\partial\xi^2}\cdot - \frac{1}{x_\xi}\frac{\partial}{\partial\xi}u^n\cdot - \mu\frac{x_{\xi\xi}}{x_\xi^3}\frac{\partial}{\partial\xi}\cdot\right]\right\}\Delta u$$

$$= -\Delta\tau\left[\frac{1}{x_\xi}\frac{\partial f^n}{\partial\xi} + \mu\frac{x_{\xi\xi}}{x_\xi^3}\frac{\partial u^n}{\partial\xi} - \frac{\mu}{x_\xi^2}\frac{\partial^2 u^n}{\partial\xi^2}\right] \qquad (2)$$

where $\beta = 1$ yields Euler implicit time differencing and $\beta = 1/2$ yields trapezoidal time differencing. Conventional central-difference approximations are used interior to both fine and coarse meshes. However, at the intermesh point where $x = 1 - \delta$ (see Fig. 5), a special formula must be applied for the derivative approximations. This is derived as follows. Consider a transformation from computational space back to physical space into an arc length variable such that

$$\frac{\partial}{\partial\xi} = \frac{\partial s}{\partial\xi}\frac{\partial}{\partial s}$$

where s is arc length along the ξ direction. Note that this mapping can be performed locally at $x = 1 - \delta$ from either the fine mesh computational system or the coarse mesh system. The $\partial/\partial s$ derivative is then approximated using a second-order accurate formula for an unequally spaced grid. The factor $\partial s/\partial\xi$ simply makes the difference approximation consistent with whichever grid the $\partial/\partial\xi$ is meant to apply to. Of particular importance is the fact that this procedure will work on a multidimensional problem provided continuity of slope across interfaces exists for all grid lines. Second derivatives in computational space transform back to arc length dependence

according to

$$\frac{\partial^2}{\partial \xi^2} = \left(\frac{\partial s}{\partial \xi}\right)^2 \frac{\partial^2}{\partial s^2} + \frac{\partial^2 s}{\partial \xi^2} \frac{\partial}{\partial s}$$

The arc length derivatives are differenced according to

$$\frac{\partial^2 (\cdot)}{\partial s^2} = \frac{2}{\Delta + \nabla} \left[\frac{\Delta(\cdot)}{\Delta} - \frac{\nabla(\cdot)}{\nabla}\right] \tag{3}$$

$$\frac{\partial (\cdot)}{\partial s} = \frac{1}{\Delta + \nabla} \left[\frac{\nabla}{\Delta} \Delta(\cdot) + \frac{\Delta}{\nabla} \nabla(\cdot)\right] \tag{4}$$

where Δ, ∇ refer to conventional forward and backward difference operators, respectively, and Δ, ∇ alone indicate operation on the arc length parameter, s. For example, $\Delta = \Delta s = s_{j+1} - s_j$. The factors $\partial s/\partial \xi$ and $\partial^2 s/\partial \xi^2$ are approximated by one-sided finite differences using the arc length data on whichever side is appropriate.

The result of the procedure just outlined, insofar as the tridiagonal algorithm is concerned, is simply a modification to the algebraic equation corresponding to the intermesh point. This requires a change in the row of the tridiagonal matrix corresponding to this point. Also, the right-hand side derivatives at this point must be differenced according to the procedures just discussed. Let point p be the intermesh point. Then p + 1 is in the fine mesh and p - 1 is in the coarse mesh. The difference scheme represented by Eq. (2) is represented at this point as

$$a_p \Delta u_{p-1} + b_p \Delta u_p + c_p \Delta u_{p+1} = r_p$$

where

$$r_p = -\Delta\tau\left\{\frac{\delta^*_\xi}{x^*_\xi}\frac{1}{\Delta+\nabla}\left(\frac{\nabla}{\Delta}\Delta f^n + \frac{\Delta}{\nabla}\nabla f^n\right) + \mu_p\frac{x^*_{\xi\xi}\delta^*_\xi}{x^{*3}_\xi}\frac{1}{\Delta+\nabla}\left(\frac{\nabla}{\Delta}\Delta u^n + \frac{\Delta}{\nabla}\nabla u^n\right)\right.$$

$$\left. - \frac{\mu_p}{x^{*2}_\xi}\left[\delta^{*2}_\xi\frac{2}{\Delta+\nabla}\left(\frac{\Delta u^n}{\Delta} - \frac{\nabla u^n}{\nabla}\right) + \delta^*_{\xi\xi}\frac{1}{\Delta+\nabla}\left(\frac{\nabla}{\Delta}\Delta u^n + \frac{\Delta}{\nabla}\nabla u^n\right)\right]\right\}$$

$$a_p = -\beta\Delta\tau\left\{\frac{\mu_p}{x^{*2}_\xi}\left[\delta^{*2}_\xi\frac{2}{(\Delta+\nabla)\nabla} - \delta^*_{\xi\xi}\frac{\Delta}{(\Delta+\nabla)\nabla}\right] + \frac{\delta^*_\xi}{x^*_\xi}u^n_{p-1}\frac{\Delta}{(\Delta+\nabla)\nabla}\right.$$

$$\left. + \frac{\mu_p x^*_{\xi\xi}}{x^{*3}_\xi}\delta^*_\xi\frac{\Delta}{(\Delta+\nabla)\nabla}\right\}$$

$$b_p = 1 - \beta\Delta\tau\left\{\frac{-\mu_p}{x^{*2}_\xi}\left[\delta^{*2}_\xi\frac{2}{\Delta+\nabla}\left(\frac{1}{\Delta}+\frac{1}{\nabla}\right) + \delta^*_{\xi\xi}\frac{1}{\Delta+\nabla}\left(\frac{\nabla}{\Delta}-\frac{\Delta}{\nabla}\right)\right]\right.$$

$$\left. + \frac{\delta^*_\xi}{x^*_\xi}\frac{u^n_p}{\Delta+\nabla}\left(\frac{\nabla}{\Delta}-\frac{\Delta}{\nabla}\right) + \frac{\mu_p}{x^{*3}_\xi}x^*_{\xi\xi}\delta^*_\xi\frac{1}{\Delta+\nabla}\left(\frac{\nabla}{\Delta}-\frac{\Delta}{\nabla}\right)\right\}$$

and

$$c_p = -\beta\Delta\tau\left\{\frac{\mu_p}{x^{*2}_\xi}\left[\delta^{*2}_\xi\frac{2}{(\Delta+\nabla)\Delta} + \delta^*_{\xi\xi}\frac{\nabla}{(\Delta+\nabla)\Delta}\right] - \frac{\delta^*_\xi}{x^*_\xi}u^n_{p+1}\frac{\nabla}{(\Delta+\nabla)\Delta}\right.$$

$$\left. - \frac{\mu_p x^*_{\xi\xi}}{x^{*3}_\xi}\delta^*_\xi\frac{\nabla}{(\Delta+\nabla)\Delta}\right\}$$

where superscript * indicates that the quantity is evaluated with a one-sided difference approximation or a selected side of the intermesh boundary. The star quantities must all be evaluated on the same side for consistency of the equation although which side is selected is optional.

This intermesh differencing was employed and various test cases were run. The results demonstrated that this concept is a valid one. Figure 6 illustrates the steady-state error distribution for the case $\mu = 0.2$, $\delta = 0.2$.

using the Euler implicit scheme ($\beta = 1$) at a Courant number of 10. Various values of μ and δ were used and the results didn't differ appreciably from those shown so long as $\mu \geq 0.1$ and no adverse clustering was used in either of the fine or coarse mesh regions. Adverse clustering is defined as follows. Define $\Delta_c = (1 - \delta)/N_c$ and $\Delta_f = \delta/N_f$ where N_c, N_f represent the number of mesh intervals in the coarse and fine mesh, respectively. Next, form the ratio $R = \Delta_f/\Delta_c$. Clustering in either region which causes

$$\frac{x_{p+1} - x_p}{x_p - x_{p-1}} < R$$

is defined as adverse clustering. This type of clustering caused the error distribution to grow but was not of concern since such adverse clustering is not used in practice. Finally, solutions could not be obtained for $\mu < 0.1$ no matter what Courant number was used. This was true even for the limiting case of $\delta = 0.5$ and $N_c = N_v$ which corresponds to an equally spaced mesh over the entire domain. Thus, it was shown that this problem was unrelated to the new operators for unequally spaced grids. It is suspected that this problem is a result of using central differences for convective terms when the effective Reynolds number is sufficiently large (μ sufficiently small).

Summarizing this section, the concept of unequally spaced operators was introduced and tested on a model equation. The results of this test prove the feasibility of the concept. The remaining sections expand the idea to the tubular projectile problem.

III. GRID GENERATION

Figure 3 illustrates the new modularized grid system to be employed. The actual generation of the grid is accomplished with a hyperbolic grid generation scheme as described in Ref. 3. The first step is to generate the fine grid for Region 1 with this generator. The grid for Region 1 is marched out a distance sufficient that this grid contains the entire boundary layer. The outer boundary of Region 1 then serves as a portion of the upper boundary of Region 3 and the lower boundary of Region 2. The grid line emanating from the projectile leading edge is constrained to be horizontal and is extended to the inflow boundary. This line separates Regions 2 and 3 forward of the fine mesh boundary. The grid for Region 2 is then generated from the starting line consisting of the straight section forward of the fine mesh continued by the upper portion of the outer boundary of the fine mesh. This starting line is marched up to a distance above the projectile of a few chord lengths. The grid for Region 3 is obtained in a similar fashion except that the starting line is marched down until every point corresponding to the last ζ = constant line is below the projectile centerline. Then the points along each ξ = constant line are adjusted along this curve so that the last ζ = constant line coincides with the projectile centerline. The orthogonal nature of this grid generator provides the needed slope continuity condition across the intermesh boundaries. It should be noted that the grid in Region 3 is not quite orthogonal after the readjustment process to fit the grid to the projectile centerline; however, it is nearly so in practice. An actual grid generated with this scheme is shown in Fig. 7.

Application of the implicit approximate-factored integration scheme to a grid system such as the one shown in Fig. 7 (schematic in Fig. 3) is far

from arbitrary. There exists a special sequence (not unique) of operations which taken together result in the final solution on the existing grid system. The structure of the sequence chosen for the present study and some motivation for this choice is the subject of the next section.

IV. INTEGRATION SCHEME TOPOLOGY

The integration scheme used may be represented as

$$\Omega_1 \Omega_2 \Delta Q = \text{RHS}$$

where Ω_1, Ω_2 are the factored finite-difference operators in the two computational coordinate directions. The order in which the directions appear is arbitrary but this choice can be made to result in easier application of boundary conditions. In this study it was necessary to solve $\Omega_\xi \Omega_\zeta \Delta Q = \text{RHS}$ in some regions and $\Omega_\zeta \Omega_\xi \Delta Q = \text{RHS}$ in others for simplicity. In general, the solution algorithm consists of four major steps:

1. Given Q^n, compute RHS.
2. Solve $\Omega_1 U^* = \text{RHS}$ for U^* by inverting block tridiagonal system.
3. Solve $\Omega_2 \Delta Q = U^*$ for ΔQ by inverting block tridiagonal system.
4. Compute new Q by $Q^{n+1} = Q^n + \Delta Q$.

Steps 2 and 3 involve the ξ and ζ direction operators which, as mentioned, may appear in either order. The application of the integration scheme to the tubular projectile problem with the present modularized grid involves proper sequencing of the ξ and ζ inversions. This is best described by itemizing each step. (Refer to Fig. 8.)

1. Perform the ξ-inversion on <u>interior</u> of Region 3.

   Solve $\Omega_\xi U^* = \text{RHS}$ for $U^* = \Omega_\zeta \Delta Q$.

2. Perform the ξ-inversion on the interior of Region 2.

   Solve $\Omega_\xi U^* = RHS$ for $U^* = \Omega_\zeta \Delta Q$.

3. Perform the ξ-inversion in Region 1. (Include outer boundary.)

   Solve $\Omega_\xi U^* = RHS$ for $U^* = \Omega_\zeta \Delta Q$.

4. Perform the ξ-inversion along the forward cut (leading edge grid line) from inflow boundary to the projectile leading edge (line AC).

5. Perform the ξ-inversion along the trailing edge cut. (See line DE of Fig. 8.)

6. Perform the ζ-inversion for leading edge region 'a' (from H to I). (Solve $\Omega_\zeta \Delta Q = U^*$ for ΔQ.)

7. Perform the ζ-inversion for leading edge cut in the fine mesh. This is region 'b'.

8. Perform the ζ-inversion for region 'c' above the projectile.

9. Perform the ζ-inversion for region 'd' below the projectile.

10. Perform the ζ-inversion for region 'e,' the trailing edge region.

The remaining portion of this section serves as an explanation of the ten steps involved in taking one integration step on this modular grid. Steps 1 and 2 are self-explanatory except to say that line ABG for Step 1 and line ABF for Step 2 are excluded from the ξ-inversion at this point. Step 3 involves the ξ-inversion around the projectile including the outer boundary of Region 1 (GBF). Note that when the intermesh boundaries are involved, a reference side must be selected for computing the geometric data (metrics, Jacobian, etc.) and, in this case, the reference side is taken to be the Region 1 side. Step 4 does a ξ-inversion along the leading edge line from

the inflow boundary to the projectile. Since in the fine mesh this computational direction is actually the negative ζ direction, the metrics--$(\zeta_x, \zeta_y, \zeta_z)$ must be used for (ξ_x, ξ_y, ξ_z) during this inversion when working in Region 1. Note that for this inversion there is a sudden change in the grid. As a result, at this interface point between the fine and coarse mesh, special differencing is required as discussed in relation to the model problem presented earlier. This is further discussed in the next section. Step 5 does the ξ-inversion along the trailing edge cut. This, of course, involves the evaluation of the RHS along the intermesh boundary which requires special difference operators in the ζ-direction. At this point, all ξ-inversions are complete. Step 6 performs a vertical inversion in region 'a' taking vertically up to be the positive computational coordinate. Since this is opposite to the actual ζ-direction in Region 3 the ζ-metrics in Region 3 must be scaled by -1 for this inversion. Note that again this sweep is through an intermesh boundary. Following Step 6, ΔQ is known in region 'a,' which includes point L. This value of ΔQ is required for Step 7 which performs the ζ-inversion for the leading edge cut in the fine mesh only. This ΔQ serves as a known boundary condition for the ζ-inversion of Step 7. The result of Step 7 is to generate ΔQ along the leading edge cut in the fine mesh (region 'b'). Step 8 performs a ζ-inversion from body to outer boundary in region 'c' above the projectile. Again an intermesh boundary is crossed in this inversion. Step 9 performs a ζ-inversion from body to projectile centerline (region 'd'). This step also involves an intermesh boundary. Step 10 involves a ζ-inversion from the projectile centerline vertically up to the outer boundary of Region 2 (region 'e').

Note that this inversion crosses three intermesh boundaries. The inversion direction is opposite of the actual ζ-direction in Region 3 and the lower part of Region 1 so the metrics again must be scaled by -1 in these regions. Following these 10 steps and the application of boundary conditions at the projectile surface and the outflow boundaries, the value of ΔQ is known everywhere. Thus, an integration step can be completed.

The next section deals with the actual intermesh operators employed.

V. INTERMESH OPERATORS

This section details the approach for performing an inversion across an intermesh boundary. Special differencing is required for convective terms, viscous terms and smoothing terms. Each of these is discussed in a general setting.

A. Convective Terms

A typical convective term for the strong-conservation-law form of the governing equations can be expressed as

$$(G\phi)_\alpha$$

where α represents one of the computational coordinates, G represents geometry related information such as combinations of metrics and Jacobian, and ϕ represents the physical flow quantity. Consider the application of such a term at an intermesh point, p, as shown in Fig. 9. Express this term as

$$(G\phi)_\alpha = G_\alpha\phi + G\delta_\alpha\phi_\delta$$

where δ is the arc length along the coordinate line. In general ϕ is continuous across the interface but G is not. As a result, G_α and δ_α are evaluated with one-sided finite differences on whichever side is taken to

be the reference. This choice is arbitrary so long as the same choice is made for all terms in the equation. ϕ is evaluated at point p and ϕ_δ is approximated by the second-order accurate formula

$$\phi_\delta \simeq a\,\phi_{p-1} + b\,\phi_p + c\,\phi_{p+1} \tag{5}$$

where

$$a = -\frac{\Delta}{\nabla(\Delta + \nabla)}\,, \qquad b = -\frac{\nabla - \Delta}{\Delta\nabla}\,, \qquad c = \frac{\nabla}{\Delta(\Delta + \nabla)}$$

Thus the result for the convective term is

$$(G\phi)_\alpha = (G\delta_\alpha a)\phi_{p-1} + (G_\alpha + G\delta_\alpha b)\phi_p + (G\delta_\alpha c)\phi_{p+1}$$

which retains tridiagonal structure.

B. Viscous Terms

A typical viscous term may be generally expressed as

$$(\mu\, G\, \phi_\alpha)_\alpha$$

where G,ϕ are as before and μ represents a viscosity or conductivity factor. This expression can be transformed to an arc length derivative as

$$(\mu\, G\, \phi_\alpha)_\alpha = [\mu_\delta \delta_\alpha^2 G + \mu\delta_\alpha G_\alpha + \mu G\delta_{\alpha\alpha}]\phi_\delta + [\mu G\delta_\alpha^2]\phi_{\delta\delta} \tag{6}$$

The factors δ_α, G_α, $\delta_{\alpha\alpha}$ are all evaluated with one-sided finite differences. μ_δ and ϕ_δ are approximated by the same formula used for the convective term example. $\phi_{\delta\delta}$ is approximated by the second-order accurate formula.

$$\phi_{\delta\delta} \simeq d\,\phi_{p-1} + e\,\phi_p + f\,\phi_{p+1} \tag{7}$$

where

$$d = \frac{2}{\nabla(\Delta + \nabla)}\,, \qquad e = -\frac{2}{\Delta\nabla}\,, \qquad f = \frac{2}{\Delta(\Delta + \nabla)}$$

The result of these one-sided formulas gives

$$(\mu\ G\ \phi_\alpha)_\alpha = [(G\delta_\alpha^2\alpha)\mu_{p-1} + (G\delta_\alpha^2 b + G_\alpha\delta_\alpha + G\delta_{\alpha\alpha})\mu_p + (G\delta_\alpha^2 c)\mu_{p+1}](a\phi_{p-1} + b\phi_p + c\phi_{p+1})$$

$$+ (\mu G\delta_\alpha^2)(d\phi_{p-1} + e\phi_p + f\phi_{p+1})$$

which again is consistent with the required tridiagonal structure. All of the viscous terms have this form and are treated in this fashion at the intermesh boundaries.

C. Smoothing Terms

The Beam-Warming algorithm does not operate effectively without added smoothing terms. The needed presence of these terms requires interface operators for them, too. On the implicit or left-hand side of the equations, a second-order smoothing term is employed. This term is identical in form to the typical viscous term, Eq. (6), with μ replaced by 1. Thus, no further discussion of this term is needed. On the right-hand side of the equations, a fourth-order smoothing term is employed. On the interior of a region (i.e., at point i = j or k in Fig. 9), this term has the form

$$\Delta\alpha^4 \frac{\partial^4\phi}{\partial\alpha^4} = \phi_{i+2} + \phi_{i-2} - 4\phi_{i+1} - 4\phi_{i-1} + 6\phi_i \tag{8}$$

where ϕ is the conservative dependent variable vector unscaled by the transformation Jacobian. This term may be expressed as

$$\Delta\alpha^4 \frac{\partial^2}{\partial\alpha^2}(\phi_{\alpha\alpha}) = \Delta\alpha^2(\phi_{\alpha\alpha_{i+1}} + \phi_{\alpha\alpha_{i-1}} - 2\phi_{\alpha\alpha_i})$$

where

$$\Delta\alpha^2\phi_{\alpha\alpha_\ell} = \phi_{\ell+1} + \phi_{\ell-1} - 2\phi_\ell$$

when ℓ = i+1, i-1, and i. Although this is perfectly equivalent to Eq. (8)

when applied to points other than p-1, p, and p+1, this formula provides a mechanism for making a consistent fourth order smoothing across the interface boundary. For example, if applied to point p-1, the result is

$$\Delta\alpha^2(\phi_{\alpha\alpha_p} + \phi_{\alpha\alpha_{p-2}} - 2\,\phi_{\alpha\alpha_{p-1}})$$

where

$$\Delta\alpha^2\phi_{\alpha\alpha_{p-2}} = \phi_{p-3} + \phi_{p-1} - 2\phi_{p-2}$$

$$\Delta\alpha^2\phi_{\alpha\alpha_{p-1}} = \phi_{p-2} + \phi_p - 2\phi_{p-1}$$

and $\phi_{\alpha\alpha_p}$ is determined just as in Eq. (6) with $\mu = G = 1$ with the result

$$\phi_{\alpha\alpha_p} = \delta_{\alpha\alpha}\phi_\delta + \delta_\alpha^2\phi_{\delta\delta}$$

where ϕ_δ and $\phi_{\delta\delta}$ are differenced according to Eqs. (5) and (7), respectively. Note that $\delta_{\alpha\alpha}$ and δ_α must be evaluated with one-sided differences on the left of the interface in this case. An identical approach is used to evaluate the smoothing term at point p+1. That is, use

$$\Delta\alpha^2(\phi_{\alpha\alpha_{p+2}} + \phi_{\alpha\alpha_p} - 2\phi_{\alpha\alpha_{p+1}})$$

where

$$\Delta\alpha^2\phi_{\alpha\alpha_{p+2}} = \phi_{p+3} + \phi_{p+1} - 2\phi_{p+2}$$

$$\Delta\alpha^2\phi_{\alpha\alpha_{p+1}} = \phi_{p+2} + \phi_p - 2\phi_{p+1}$$

and $\phi_{\alpha\alpha_p}$ is determined as before except that $\delta_{\alpha\alpha}$ and δ_α must be evaluated on the right of the interface.

The only remaining task is to determine the smoothing term applicable

at point p. This is done by satisfying a global conservative property (see Ref. 4) along the typical grid line indicated in Fig. 9. This requires that the sum of the smoothing terms at all the points along this line equals zero. Let S represent the smoothing term of interest. Then S_ℓ for $\ell = p-3,\ldots,p+3$ becomes

$$S_{p-3} = \phi_{p-5} - 4\phi_{p-4} + 6\phi_{p-3} - 4\phi_{p-2} + \phi_{p-1}$$

$$S_{p-2} = \phi_{p-4} - 4\phi_{p-3} + 6\phi_{p-2} - 4\phi_{p-1} + \phi_p$$

$$S_{p-1} = \phi_{p-3} - 4\phi_{p-2} + \alpha_L\phi_{p-1} - \beta_L\phi_p + \gamma_L\phi_{p+1}$$

$$S_p = \phi_{p-2} + (3 - \alpha_L - \gamma_R)\phi_{p-1} + (\beta_L + \beta_R - 2)\phi_p + (3 - \alpha_R - \gamma_L)\phi_{p+1} + \phi_{p+2}$$

$$S_{p+1} = \gamma_R\phi_{p-1} - \beta_R\phi_p + \alpha_R\phi_{p+1} - 4\phi_{p+2} + \phi_{p+3}$$

$$S_{p+2} = \phi_p - 4\phi_{p+1} + 6\phi_{p+2} - 4\phi_{p+3} + \phi_{p+4}$$

$$S_{p+3} = \phi_{p+1} - 4\phi_{p+2} + 6\phi_{p+3} - 4\phi_{p+4} + \phi_{p+5}$$

where

$$\alpha_L = 5 + \Delta\alpha^2\left(\delta_{\alpha\alpha_L} a + \delta^2_{\alpha_L} d\right)$$

$$\beta_L = 2 - \Delta\alpha^2\left(\delta_{\alpha\alpha_L} b + \delta^2_{\alpha_L} e\right)$$

$$\gamma_L = \Delta\alpha^2\left(\delta_{\alpha\alpha_L} c + \delta^2_{\alpha_L} f\right)$$

$$\alpha_R = 5 + \Delta\alpha^2\left(\delta_{\alpha\alpha_R} c + \delta^2_{\alpha_B} f\right)$$

$$\beta_R = 2 - \Delta\alpha^2\left(\delta_{\alpha\alpha_R} b + \delta^2_{\alpha_R} e\right)$$

$$\gamma_R = \Delta\alpha^2\left(\delta_{\alpha\alpha_R} a + \delta^2_{\alpha_R} d\right)$$

The constants a, b, c, d, e, f are those used in Eqs. (5) and (7). The subscripts L and R indicate on which side of the interface boundary the arc length derivatives are evaluated.

The smoothing philosophy indicated here is employed at all interface boundary points and their immediate neighbors.

VI. CONCLUDING REMARKS

The tubular projectile code has been extensively modified to incorporate an efficient grid system consisting of three distinct modules. The Beam-Warming implicit algorithm has been modified to apply to the regions of module interfaces. Feasibility of such module interfaces with discontinuous metrics was tested on a model problem with positive results. New operators were derived and employed for use at interface boundaries. These operators include applications for convective terms, viscous terms, and smoothing terms. The topology for implementation of the new factored algorithm is complex and was described in Section IV. The resulting computer code is quite different in character than the original version, though many similarities exist in its structure; its size is roughly three times the size of the original. This code currently resides on the Ballistics Research Laboratory Launch and Flight Division's VAX computer.

An extensive debugging effort still remains, following which some test cases will be computed and compared to existing data.

VII. ACKNOWLEDGEMENT

This report summarizes work performed on Delivery Order No. 0218 of a Scientific Services Agreement between Battelle Columbus Laboratories and the author and authorized under Contract DAAG29-81-D-0100 by the United States Army. The work was performed between 1 April, 1982 and 30 March 1983.

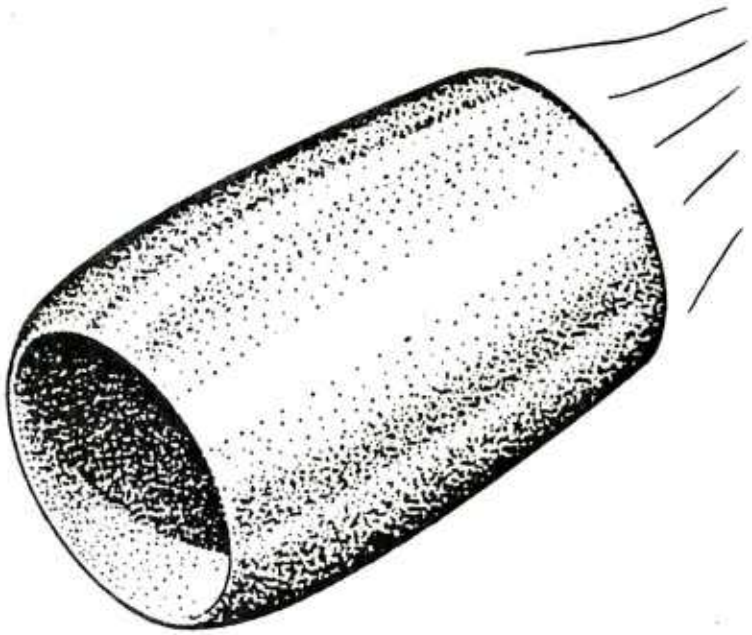

Figure 1. Hollow Projectile

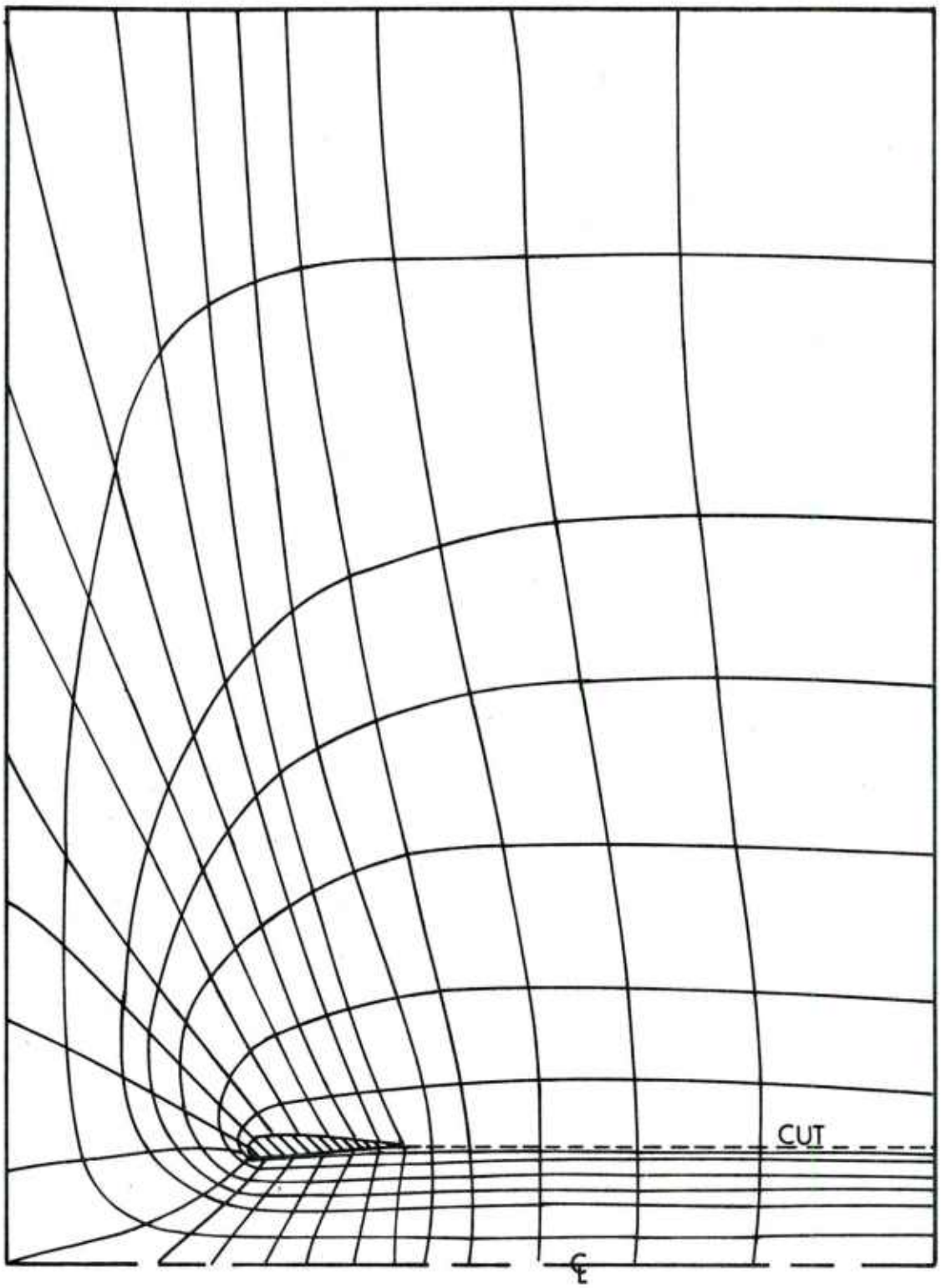

Figure 2. Typical C-Grid for Hollow Projectile Problem

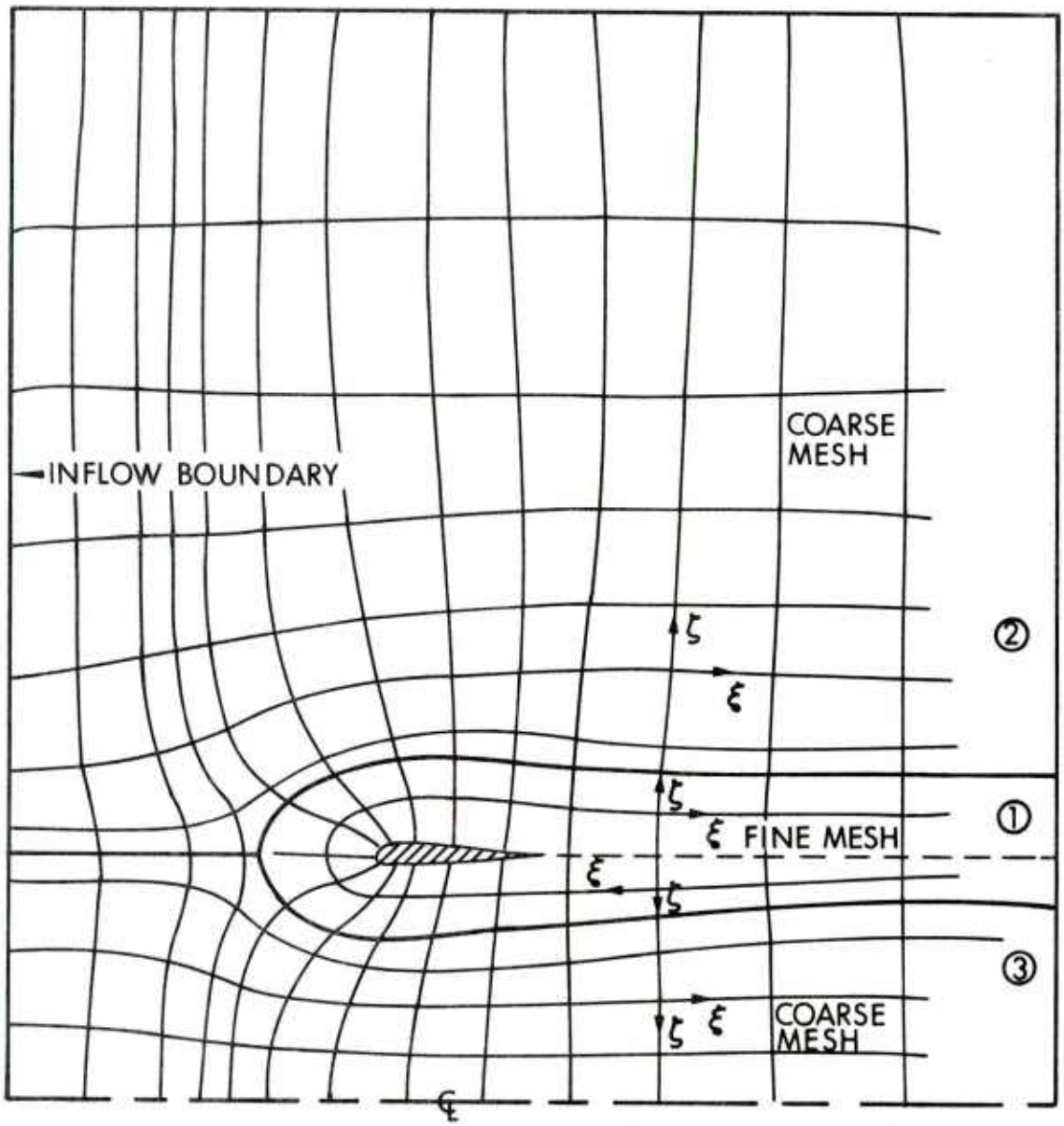

Figure 3. Schematic of New Grid System

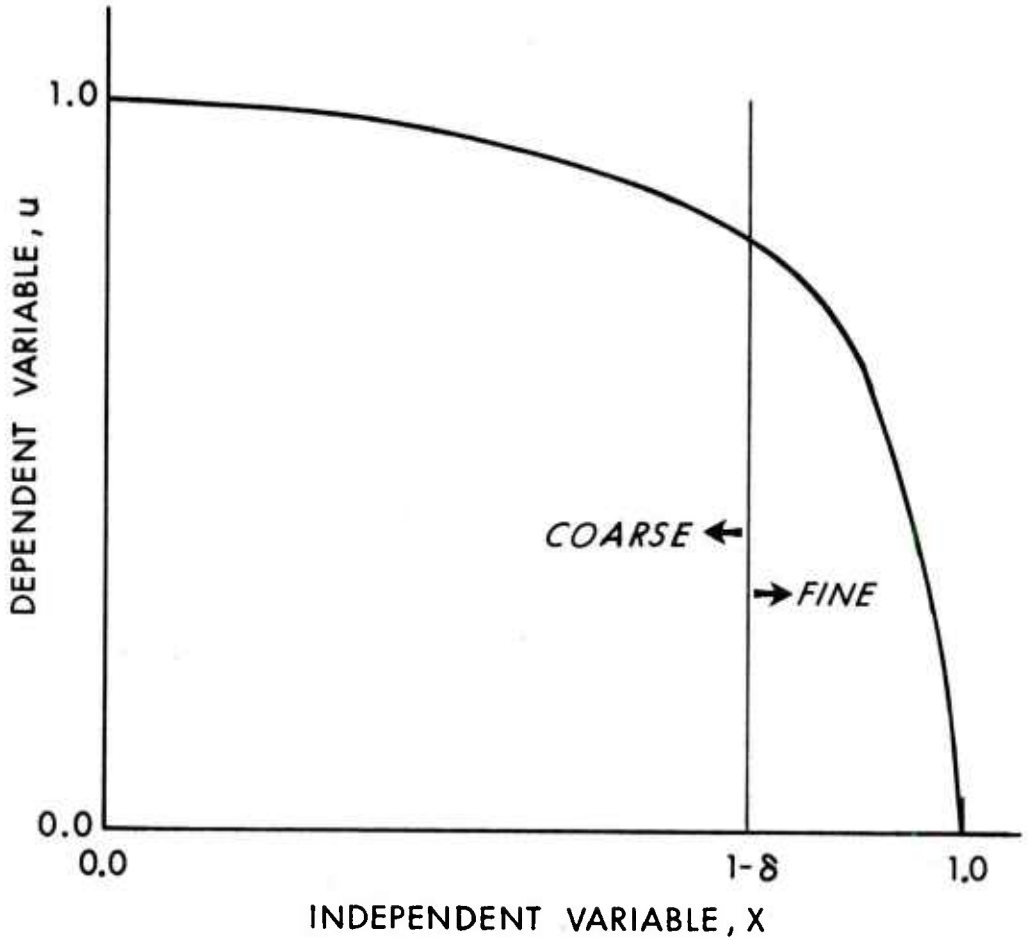

Figure 4. Typical Solution of Nonlinear Viscous Burgers' Equation

Figure 5. Dual Mesh for Concept Testing

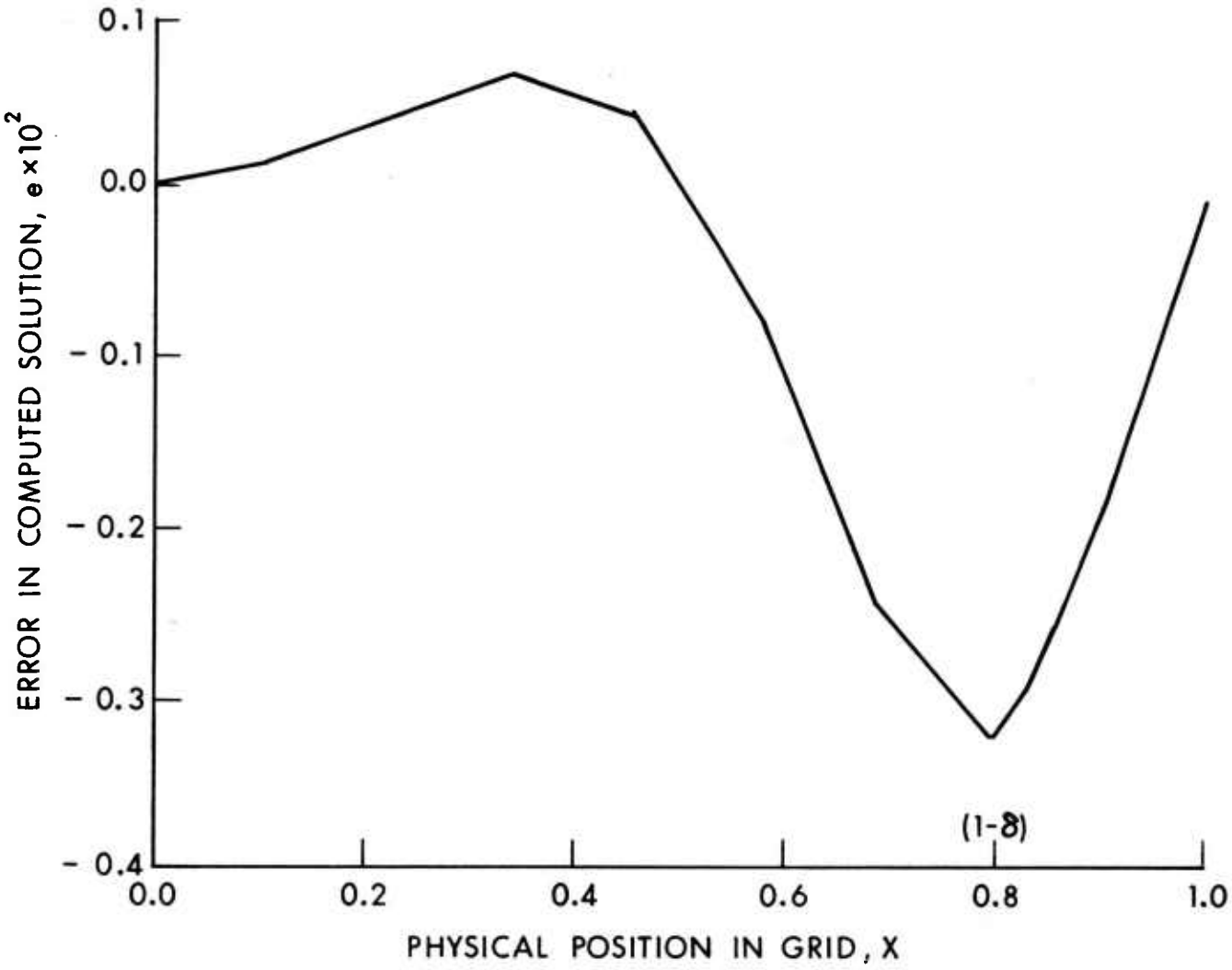

Figure 6. Error Distribution in Computed Solution to Test Equation for $\mu = 0.2$, $\delta = 0.2$, $\beta = 1.0$

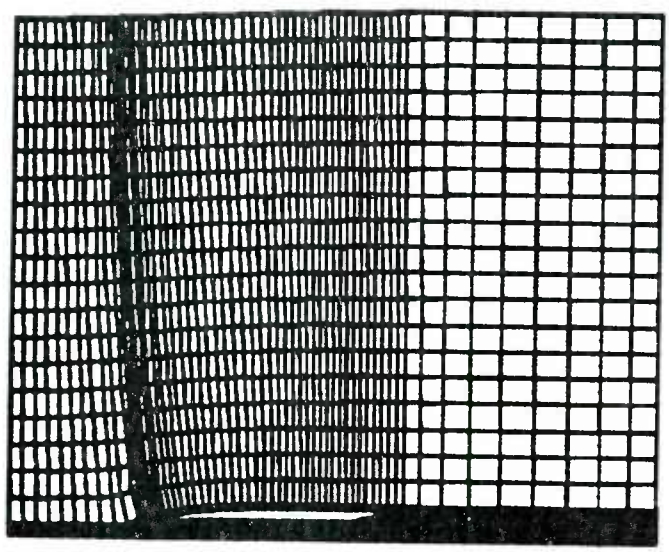

Figure 7. Actual Grid System for a Sharp Leading and Trailing Edge Hollow Projectile

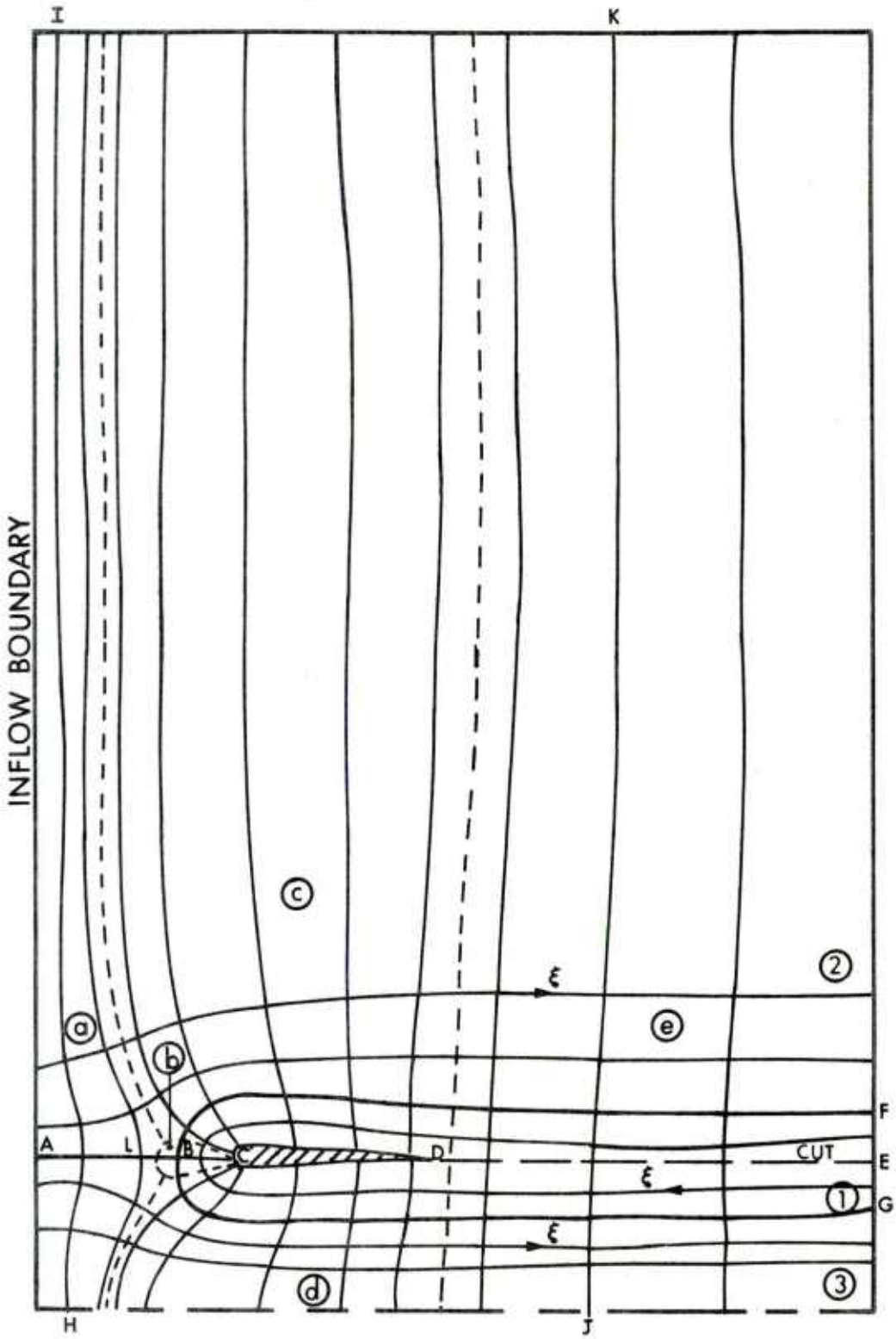

Figure 8. Integration Scheme Topology

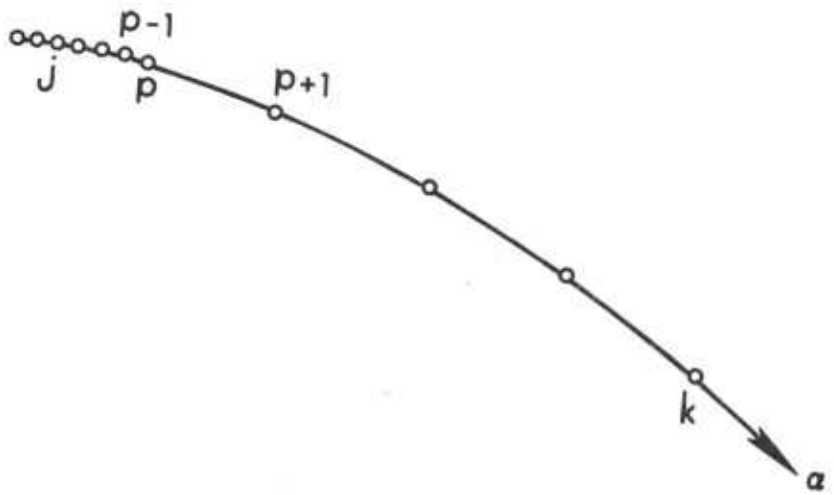

Figure 9. Arbitrary Coordinate Line Through an Intermesh Boundary

REFERENCES

1. C.J. Nietubicz, T.H. Pulliam, and J.L. Steger, "Numerical Solution of the Azimuthal-Invariant Thin-Layer Navier-Stokes Equations," AIAA Paper 79-0010, January 1979.

2. R.M. Beam and R.F. Warming, "An Implicit Factored Scheme for the Compressible Navier-Stokes Equations," AIAA Journal, Vol. 16, No. 4, April 1978, pp. 393-402.

3. C.J. Nietubicz, K.R. Heavey, and J.L. Steger, "Grid Generation Techniques for Projectile Configurations," Proceedings of the 1982 Army Numerical Analysis and Computers Conference, ARO Report 82-3.

4. R.F. Warming and R.M. Beam, "Upwind Second-Order Difference Schemes and Applications in Unsteady Aerodynamic Flows," Proc. AIAA 2nd Computational Fluid Dynamics Conference, Hartford, Connecticut, June 1975, pp. 17-28.

DISTRIBUTION LIST

No. of Copies	Organization
12	Administrator Defense Technical Info Center ATTN: DTIC-DDA Cameron Station Alexandria, VA 22314
1	Commander US Army Materiel Development and Readiness Command ATTN: DRCDMD-ST 5001 Eisenhower Avenue Alexandria, VA 22333
7	Commander Armament Research and Development Center US Army Armament, Munitions and Chemical Command ATTN: DRSMC-TDC (D) DRSMC-TSS (D) DRSMC-LCA-F (D) Mr. D. Mertz Mr. A. Loeb Mr. H. Hudgins Mr. E. Friedman Dover, NJ 07801
1	Commander US Army Armament, Munitions and Chemicals Command ATTN: DRSMC-LEP-L (R) Rock Island, IL 61299
1	Director Armament Research and Development Center Benet Weapons Laboratory US Army Armament, Munitions and Chemical Command ATTN: DRSMC-LCB-TL Watervliet, NY 12189
1	Commander US Army Aviation Research and Development Command ATTN: DRDAV-E 4300 Goodfellow Blvd. St. Louis, MO 63120
1	Director US Army Air Mobility Research and Development Laboratory Ames Research Center Moffett Field, CA 94035
1	Commander US Army Communications Rsch and Development Command ATTN: DRSEL-ATDD Fort Monmouth, NJ 07703
1	Commander US Army Electronics Research and Development Command Technical Support Activity ATTN: DELSD-L Fort Monmouth, NJ 07703
3	Commander US Army Missile Command ATTN: DRSMI-R DRSMI-RDK Mr. R. Deep Redstone Arsenal, AL 35898
1	Commander US Army Missile Command ATTN: DRSMI-YDL Redstone Arsenal, AL 35898
1	Commander US Army Tank Automotive Command ATTN: DRSTA-TSL Warren, MI 48090
1	Director US Army TRADOC Systems Analysis Activity ATTN: ATAA-SL White Sands Missile Range NM 88002
1	Commander US Army Research Office P. O. Box 12211 Research Triangle Park NC 27709

DISTRIBUTION LIST

No. of Copies	Organization
1	Commander US Naval Air Systems Command ATTN: AIR-604 Washington, D. C. 20360
2	Commander US Naval Surface Weapons Center ATTN: Dr. F. Moore Dr. P. Daniels Dahlgren, VA 22448
3	Commander US Naval Surface Weapons Center ATTN: Code 312 Dr. W. Yanta Mr. R. Voisinet Code R44 Dr. R. U. Jettmar Silver Spring, MD 20910
1	Commander US Naval Weapons Center ATTN: Code 3431, Tech Lib China Lake, CA 93555
1	Director NASA Langley Research Center ATTN: NS-185, Tech Lib Langley Station Hampton, VA 23365
2	Commandant US Army Infantry School ATTN: ATSH-CD-CSO-OR Fort Benning, GA 31905
3	Director NASA Ames Research Center ATTN: MS-202A-14, Dr. P. Kutler MS-202-1, Dr. T. Pulliam MS-227-8, Dr. L. Schiff Moffett Field, CA 94035
2	Sandia Laboratories ATTN: Division No. 1331 Mr. H. R. Vaughn Mr. G. R. Eisler P.O. Box 580 Albuquerque, NJ 87115
1	AEDC Calspan Field Services ATTN: MS 600 (Dr. John Benek) AAFS, TN 37389
1	AFWL/SUL Kirtland AFB, NM 87117
1	Bendix Guided Systems Division ATTN: MS 2/17A, S. Wasserman Teterboro, NJ 07608
1	Stanford University Department of Aeronautics and Astronautics ATTN: Prof. J. Steger Stanford, CA 94305
1	University of California, Davis Department of Mechanical Engineering ATTN: Prof. H.A. Dwyer Davis, CA 95616
1	University of Delaware Mechanical and Aerospace Engineering Department ATTN: Dr. J. E. Danberg Newark, DE 19711
1	University of Iowa ATTN: R. G. Hindman RR1 Box 22 Maxwell, Iowa 50161

Aberdeen Proving Ground

Dir, USAMSAA
ATTN: DRXSY-D
DRXSY-MP, H. Cohen

DISTRIBUTION LIST

No. of Copies	Organization
	Cdr, USATECOM ATTN: DRSTE-TO-F
	Cdr, CRDC, AMCCOM ATTN: DRSMC-CLB-PA DRSMC-CLN DRSMC-CLJ-L

USER EVALUATION OF REPORT

Please take a few minutes to answer the questions below; tear out this sheet, fold as indicated, staple or tape closed, and place in the mail. Your comments will provide us with information for improving future reports.

1. BRL Report Number _____

2. Does this report satisfy a need? (Comment on purpose, related project, or other area of interest for which report will be used.)

_____

_____

_____

3. How, specifically, is the report being used? (Information source, design data or procedure, management procedure, source of ideas, etc.) _____

_____

_____

4. Has the information in this report led to any quantitative savings as far as man-hours/contract dollars saved, operating costs avoided, efficiencies achieved, etc.? If so, please elaborate.

_____

_____

5. General Comments (Indicate what you think should be changed to make this report and future reports of this type more responsive to your needs, more usable, improve readability, etc.) _____

_____

_____

_____

6. If you would like to be contacted by the personnel who prepared this report to raise specific questions or discuss the topic, please fill in the following information.

Name: _____

Telephone Number: _____

Organization Address: _____

_____

_____